



Characterization of the lithium concentration and distribution as a function of depth for alumina coatings after exposure to PbLi

R. González-Arrabal^{a,b,*}, E. Carella^c, F.J. Sánchez^c, G. de la Cuerda-Velázquez^{a,b}, G. García^d, J.M. Perlado^{a,b}, T. Hernández^d

^a Instituto de Fusión Nuclear Guillermo Velarde, ETSI de Industriales, Universidad Politécnica de Madrid, C/José Gutiérrez Abascal, 2, E-28006, Madrid, Spain

^b Departamento de Ingeniería Energética, ETSI de Industriales, Universidad Politécnica de Madrid, C/José Gutiérrez Abascal, 2, E-28006, Madrid, Spain

^c National Fusion Laboratory, CIEMAT, Avda. Complutense 40, 28040, Madrid, Spain

^d Centro de Micro-Análisis de Materiales (CMAM), Universidad Autónoma Madrid (UAM), Campus de Cantoblanco, E-28049, Madrid, Spain

HIGHLIGHTS

- PbLi action on Al₂O₃ coatings.
- Diffused Li concentration as a function of depth for Al₂O₃ coatings immersed in LiPb under stagnant conditions.
- Combination of nuclear reactions analysis and Rutherford backscattering spectroscopy for accurate Lithium quantification.

ARTICLE INFO

Keywords:

Nuclear fusion
Breeding blanket
Corrosion barriers
Tritium barriers
Coatings
Lithium distribution
Ion beam analysis

ABSTRACT

The development of multifunctional barriers that prevent tritium leaks from the breeding blanket and corrosion of the structural steel is essential for safe, viable and cost-effective fusion reactor operation.

Al₂O₃ coatings are considered to be one of the most promising options to act as tritium permeation barrier (TPB). However, previous studies have shown that lithium from the breeding blanket penetrates into these coatings and reacts with them forming lithium aluminate phases. The diffusion of lithium into the coating may influence its performance, particularly under neutron irradiation.

In this study, we characterize the Li content and distribution as a function of depth for Al₂O₃ coatings deposited by pulsed laser deposition on EUROFER substrate after exposure to PbLi, at a constant temperature of 550 °C, for times of up to 7000 h, under stagnant conditions. We do it by using secondary ions mass spectroscopy and, a combination of ion beam analysis techniques (nuclear reaction analysis and Rutherford backscattering spectroscopy). Finally, we discuss the possible consequences of lithium diffusion in the coating performance under neutron irradiation in relation to the behavior of light species, produced out of transmutation reactions, and to the possible radiation induced change in the coating morphology.

1. Introduction

Nuclear fusion reactors, both in the magnetic and inertial confinement approaches (MCF and ICF, respectively) may rely on the use of the deuterium - tritium fusion reaction because of its high reaction cross-section which allows the easiest way to reach ignition. Deuterium exists in nature and can be extracted from water. However, tritium is unstable (with a half-life of ~ 12.3 years) and is found only in trace amounts. Therefore, the unavailability of external tritium sources demands that commercial nuclear fusion reactors must produce their own

fuel. To achieve this, the breeding blanket (BB) of the reactor in addition to recover the energy carried by the neutrons (approximately 80% of the fusion energy), must breed tritium by the conversion of lithium into tritium to replace that burnt in the fusion process. Thus, nuclear fusion reactors have to be tritium self-sufficient.

Diverse BB approaches, solid and liquid, have been suggested. One of the main problems that the liquid breeding approach faces is the corrosion of the structural steel in contact with it. In the particular case of using lithium-lead eutectic; PbLi, as BB, it has been reported that its interaction with the structural material (reduced activation ferritic-

* Corresponding author.

E-mail address: raquel.gonzalez.arrabal@upm.es (R. González-Arrabal).

<https://doi.org/10.1016/j.jnucmat.2023.154688>

Received 30 March 2023; Received in revised form 24 July 2023; Accepted 16 August 2023

Available online 23 August 2023

0022-3115/© 2023 Published by Elsevier B.V.

martensitic (RAFM) steels) leads to the dissolution of the majority of elements of the steel and the formation of intermetallic phases that can re-precipitate in the form of oxides [1]. The corrosion rate of RAFM steels in PbLi depends on temperature, velocity of the flow and magnetic field; e. g. it can reach 250 $\mu\text{m}/\text{year}$ at temperatures of 550 °C and flow velocity of 10 cm/s [2]. This fact inevitably leads to the degradation of mechanical properties of the steel. Another important factor to consider regarding corrosion is the oxygen content in the system. Oxygen is one of the most common impurities in eutectics as PbLi and PbBi. Several studies show that the presence of oxygen, even at extremely low concentrations, (approximately 1×10^{-7} wt.%), makes it difficult to find steel candidates with an acceptable corrosion rate in an un-passivated state when operating above 450 °C [3,4].

In addition to corrosion, it is important to mention that, due to transmutation reactions, under neutron irradiation tritium, T, and helium, He, are continuously produced in the BB. Considering the high permeability of T in steels in the operational temperature range [5,6], it is expected that a fraction of the produced T will penetrate in the structural steel, leading to swelling and embrittlement, and further permeating into the cooling system [7,8]. Since T is radioactive, its inventory in the reactor needs to be controlled and kept below a certain limit. Because of that, its permeation to reactor coolant systems has to be minimized. Thus, in order to avoid corrosion problems and to fulfill regulatory requirements, specially thinking in the demonstration power station (DEMO) scenario, operating in a continuous mode, the structural walls made of EUROFER have to be coated with tritium permeation barriers (TPBs) [9].

The general characteristics of tritium permeation barriers must include: (i) ability to prevent or highly reduce hydrogen adsorption; (ii) high permeation reduction factors (PRFs); (iii) high performance in relation to irradiation, (iv) low activation, (v) high thermomechanical integrity, (vi) PbLi compatibility, (vii) good adhesion to the substrate and, in the case of MCF, (viii) low electrical conductivity.

During the last years, several efforts have been made to select the best TPB candidate. Several metal-oxides, nitrides, or carbides have been produced by diverse methods to be used as TPBs [10–19]. So far, Al_2O_3 coatings are suggested as one of the most promising TPB candidates [20]. A reduction factor in the deuterium permeation through the steel of about 1000 was reported for irradiated Al_2O_3 coated steel compared to bare material in the temperature range close to 450 °C [21]. However, recent studies pointed out that when being in contact with the BB at relevant operation temperatures, Li penetrates along the whole Al_2O_3 coating thickness and reacts with it forming lithium aluminate phases [19]. The formation of lithium aluminate from different compounds containing aluminum and lithium is relatively simple and has been already reported in the literature [22–24]. However, to the best of our knowledge the presence of Li in Al_2O_3 coatings has been neither quantified nor studied in detail so far. One possible reason for that is the difficulty to detect light elements, especially if an accurate quantification is needed, by using conventional materials characterization techniques.

In the following, we mention some experimental techniques suitable for Li characterization highlighting its capabilities and limitations. Secondary ion mass spectrometry (SIMS) allows measuring the Li depth distribution, but quantification is only possible with the use of suitable standards [25]. X-ray photoelectron spectroscopy (XPS) also allows measuring Li, but it does not allow to characterize accurately concentration profiles for thick layers [26]. Atom probe tomography (APT) also allows measuring 3D Li concentration profiles, but it does only in a very small volume [27] which may not be representative for the whole sample, especially for samples with Li inhomogeneities spreading over the μm range. Within this framework, ion beam analysis (IBA) techniques are powerful tools which permit direct, non-destructive, and accurate quantitative elemental concentration characterization, including light ions such as lithium in a much larger area for samples with thickness in the μm range.

In this paper, we characterize the Li content and distribution as a function of depth for diverse Al_2O_3 coatings deposited by pulsed laser deposition (PLD) after exposure to PbLi at a constant temperature of 550 °C for times of up to 7000 h under stagnant conditions. We do it by using SIMS and a combination of IBA techniques: nuclear reaction analysis (NRA) and Rutherford backscattering spectroscopy (RBS). Then, we analyze the possible consequences of Li diffusion in those layers under neutron irradiation in relation to coating integrity, permeation reduction factor (PRF) value and, adhesion of the coating to the EUROFER substrate.

2. Experimental

We characterize amorphous and dense Al_2O_3 coatings deposited by PLD on EUROFER after exposure to PbLi under stagnant conditions at a constant temperature of 550 °C for different times (4000 h, 7000 h). Corrosion experiments were carried out at ENEA – RACHEL facility by keeping the samples in direct contact with PbLi [28]. The PbLi exposure conditions together with the sample code and thickness are listed in Table I. More details about the coating deposition procedure and coatings properties are described in [10,29]. After PbLi exposure, prior to any further characterization, the samples were cleaned with a standard chemical solution consisting on acetic acid and 5% hydrogen peroxide.

The morphological and microstructural properties of the coatings were characterized with scanning electron microscopy (SEM) and glancing-angle X-ray diffraction (GIXRD), respectively. SEM measurements were performed by using a Zeiss Auriga Compact/Bruker X Flash microscope. GIXRD spectra were measured by using a Philips X-PERT PRO MRD four cycle diffractometer equipped with a $\text{CuK}\alpha$ ($\lambda = 0.15405$ nm) radiation source. Prior to SEM characterization, a thin layer of C with a few nanometers thickness was deposited by sputtering on top of the Al_2O_3 .

The elemental composition of the coatings was characterized with SIMS and IBA techniques. SIMS measurements were carried out in a Hiden analytical Workstation. Two IBA techniques were used, in combination, NRA and RBS. By choosing an adequate experimental configuration (selected beam energy of 3.00 MeV, no foil in front of the detectors and, location of the detector to the beam direction), as in our case, the signal from these two techniques can be detected simultaneously. Measurements were performed at the standard beam line of the centre of Microanalysis of Materials (CMAM/UAM) [30]. Special attention was paid to the determination of the Li distribution as a function of depth. To do that, measurements were done following the procedure described in ref. [31] using a H beam at an energy of 3.00 MeV. For that beam energy several nuclear reaction channels are simultaneously opened. All possible channels related to Li together with the emitted nuclear reaction products, their energy and stopping power in Al_2O_3 are shown in Table II. The stopping power was calculated with the SRIM code [32] by considering a nominal Al_2O_3 density of 3.96 g/cm^3 [33]. One of the advantages of using this procedure is that it allows to characterize the lithium content from the ^4He signal coming from the $^7\text{Li}(p, ^4\text{He})^4\text{He}$ nuclear reaction, which is background free ($E_{^4\text{He}} = 7.71$ MeV) [34]. Thus, it improves the measurement sensitivity and accuracy in the characterization of the Li depth profiling. Since no foil was used in between the sample and the detector, the α -particles produced in the nuclear reaction and the backscattered protons from Li

Table I
Sample code and thickness for diverse Al_2O_3 coatings exposure to PbLi under stagnant conditions, at a temperature of 550 °C, for times of 4000 and 7000 h.

Sample code	Sample thickness (μm)	Time (h)	PbLi exposure Temperature (°C)	Conditions
S1	3	7000	550	Stagnant
S2	5	7000	550	Stagnant
S3	3	4000	550	Stagnant

Table II

Nuclear reactions taken place when bombarding Li with a H beam at an energy of 3.00 MeV, nuclear reactions products, its energy and, its stopping power in an Al_2O_3 matrix with a density of 3.96 g/cm^3 [33].

Nuclear reaction	Nuclear reaction products	Energy of the nuclear reactions products (MeV)	Stopping power in Al_2O_3 (keV/ μm)
${}^7\text{Li}(\text{p}, {}^4\text{He}){}^4\text{He}$	${}^4\text{He}$	7.71	199.73
${}^6\text{Li}(\text{p}, {}^4\text{He}){}^3\text{He}$	${}^3\text{He}$	2.41	348.17
${}^6\text{Li}(\text{p}, {}^4\text{He}){}^3\text{He}$	${}^4\text{He}$	1.53	500.62
${}^6\text{Li}(\text{p}, {}^3\text{He}){}^4\text{He}$	${}^4\text{He}$	1.53	500.62
${}^7\text{Li}(\text{p}, {}^3\text{He}){}^4\text{He}$	${}^3\text{He}$	2.41	348.27

and other elements (Fe, Al, O...) present in the Al_2O_3 coating and in the EUROFER substrate were simultaneously detected by two standard Si-barrier subtending a solid angle of $7.1 \pm 0.4 \text{ mSrad}$ and $4.1 \pm 0.1 \text{ mSrad}$ and at angles of 150° and 170° respectively to the beam direction. The beam spot and the current were selected to be $1.5 \times 1.5 \text{ mm}^2$ and $\sim 20 \text{ nA}$, respectively.

When using IBA techniques, the elemental composition of the samples was estimated by comparing experimental and simulated spectra. Simulations were performed with the commercial computer code SIMNRA [35]. For the simulation of the peaks related to lithium the cross section reported by Paneta et al. were used for the ${}^7\text{Li}(\text{p}, {}^4\text{He}){}^4\text{He}$ and for the ${}^7\text{Li}(\text{p}, \text{p}_0){}^7\text{Li}$ reactions [36]. The “chi-squared” algorithm was used to determine the goodness of the quality of the peak fit.

3. Results

Fig. 1 shows SEM images for a representative Al_2O_3 coating deposited by PLD on EUROFER substrate prior to and after the corrosion test. Prior to the corrosion test some scratches associated with the grinding process are clearly visible which indicates that the Al_2O_3 coating precisely replicates the substrate surface topology. These lines are somehow blurred but still visible after the corrosion test. The morphology of the coating remains quite stable against PbLi under the tested conditions: small color inhomogeneity, but no changes in its nominal thicknesses and no evidence of delamination. However, in agreement with other authors [22–24], x-ray diffraction measurements, shown in Fig. 2, illustrate that corrosion leads to the appearance of a series of peaks which correspond to different LiAlO_2 phases. Thus, XRD data indicate that Li has penetrated into the coatings reacting with it. However, neither the depth to which lithium has diffused nor the amount of diffused lithium can be deduced from these data.

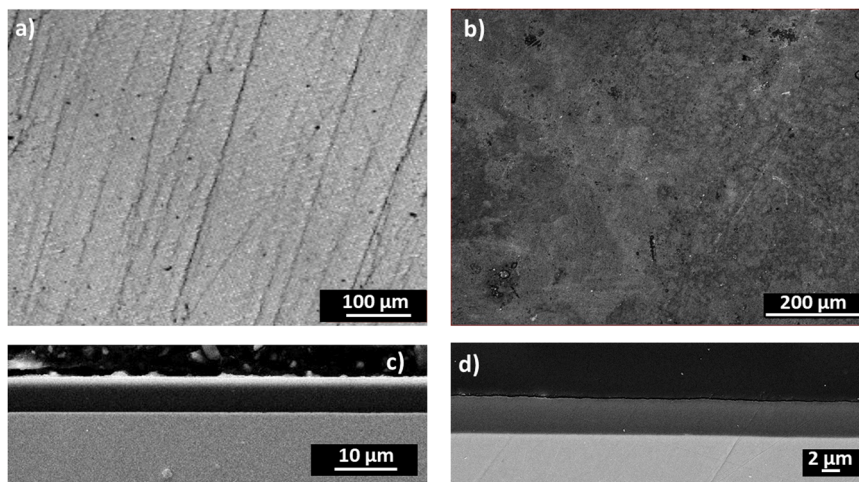


Fig. 1. Top view and cross-sectional SEM image for a representative Al_2O_3 coating deposited by PLD on EUROFER substrate prior to (a and c, respectively) and after (b and d, respectively) the corrosion test.

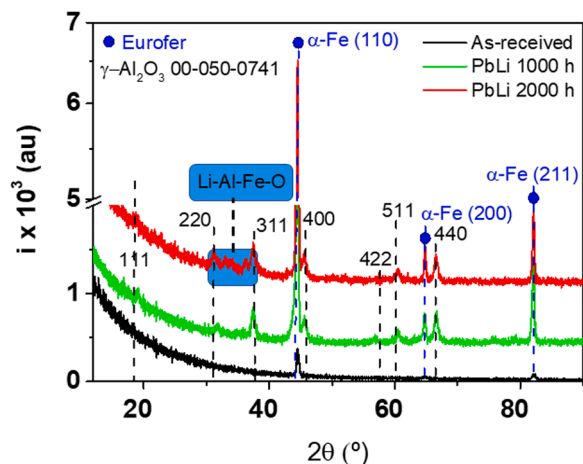


Fig. 2. X-ray diffraction patterns measured prior to and after the corrosion test for diverse Al_2O_3 coating deposited by PLD on EUROFER substrate.

Fig. 3 illustrates measured SIMS spectra for three representative Al_2O_3 coatings exposure to PbLi.

SIMS data show that Li distributes along the whole coating thickness. The Li distribution is not homogeneous along depth, but it is higher at the coating surface and at the coating-EUROFER interface. These data are further corroborated by IBA measurements. Fig. 4 shows measured and simulated ion-beam analysis spectra for the same coatings. It is important to mention that even when all the reaction channels depicted in Table II are opened simultaneously, in the spectra shown in Fig. 4, we only observe the presence of two peaks related to Li. The high energy peak (channels 1380 to 1600) corresponds to the ${}^4\text{He}$ particles coming from the ${}^7\text{Li}(\text{p}, {}^4\text{He}){}^4\text{He}$ nuclear reaction (see inset in Fig. 4) and the low energy peak (channels 240–350) corresponds to proton backscattered by Li (p_0). In principle, one could expect to also see some peaks related to the nuclear reaction taking place with ${}^6\text{Li}$. However, these peaks are not observed mainly because of two reasons: the low cross section of the nuclear reaction and the small natural abundance of ${}^6\text{Li}$ (7.5%) [37].

In agreement with SIMS data, Li is observed in all the studied coatings distributing from the coating surface to the EUROFER substrate along the whole coating thickness. A good fit of the measured spectra can be only achieved if we assume that the coating is composed of diverse layers with different Li content (see Fig. 5) which indicates that the lithium distribution along the coating is inhomogeneous. It is high at the coating surface ($\sim 12 \text{ at.}\%$), then it decreases ($\sim 10 \text{ at.}\%$) and

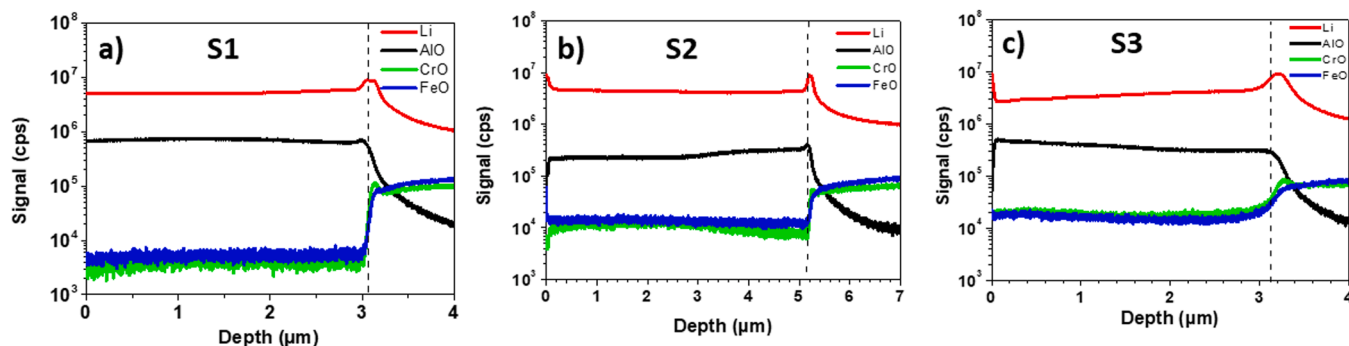


Fig. 3. SIMS spectra for three representative Al_2O_3 coatings exposure to PbLi under the conditions described in Table I.

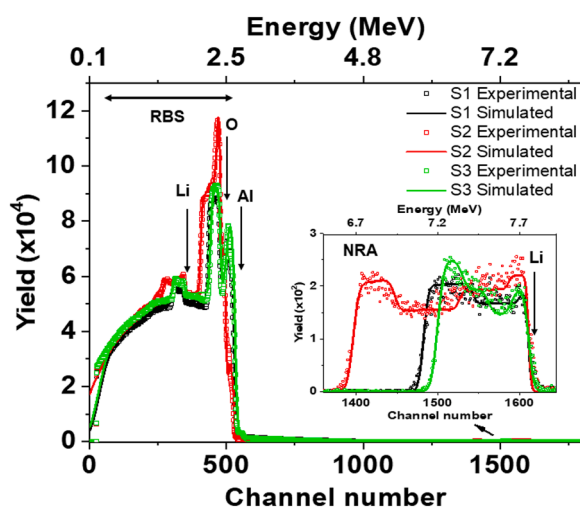


Fig. 4. Measured and simulated ion-beam analysis spectra for Al_2O_3 coatings deposited on EUROFER steels exposure to PbLi under the conditions shown in Table I.

becomes larger when reaching the coating/EUROFER interface (~ 14 at. %). For the thinnest coatings (S1 and S3), independently of the exposure time, the Li content at the coating/EUROFER interface is observed to be larger than at the coating surface whereas similar Li concentration values at those regions are observed for the thickest coating. For clarity sake, Fig. 5 shows the lithium concentration and the areal density of each particular layer in the layer scheme, regarded the optimal choice, in which the coatings have been divided to fit the measured spectra.

To study the possible diffusion of Li into the EUROFER substrate some additional simulations have been carried out by considering the presence of Li in the EUROFER substrate. Simulations were performed by assuming different Li contents (from 5 up to 14 at.% which is the maximum content calculated at the Al_2O_3 /EUROFER interface), and diffusion depths (from 1×10^{17} to 3×10^{18} at/cm²). The peak selected to monitor the possible diffusion of Li into the EUROFER is that related to the ⁴He particles, because even at that high energy (7.71 MeV), they exhibit a higher stopping power (199.73 keV/μm) than backscattered protons which emerge at an energy of 1.75 MeV (53.03 keV/μm) and therefore, they offer a better depth resolution insight (see Table II). Simulation results, for two samples with diverse thicknesses and exposure times, are shown in Fig. 6. For comparison measured data are also depicted.

We observe, for both samples regardless of its thickness, that spectra simulated for all assuming Li concentration start to deviate from experimental ones when the Li penetration depth into the EUROFER is $\sim 2 \times 10^{18}$ at/cm². These data may be considered as a first indication that, within the resolution of the selected techniques, there is no

evidence of a significant Li diffusion into the EUROFER at thickness larger than $\sim 2 \times 10^{18}$ at/cm².

4. Discussion

The first thing to be discussed is the measured Li content and its inhomogeneous distribution along the coating depth. Lithium diffusion data in Al_2O_3 are very scarce, especially when dealing with amorphous materials. Most Li diffusion, both experimental and computational, studies have been carried out within the framework of the development of advanced lithium batteries. These works show that, as many in many other diffusion processes, the Li diffusion strongly depends on material morphology and microstructure, as well as on the Li content itself [38, 39]. So far, the studies performed by combining density functional and kinetic Monte Carlo on the diffusivity of interstitial Li in amorphous α - Al_2O_3 indicate that the Li diffusivity in this material is very slow ($\sim 2.7 \times 10^{-14}$ m²s⁻¹ at 600 K) because of unfavorable Li binding sites and pretty large diffusion barriers. This Li diffusivity value is orders of magnitude lower than that for β - Al_2O_3 which has a more open structure [38]. In our particular case, we observe a quite large Li content all along the coating thickness and an increase of the Li concentration both at the EUROFER/ Al_2O_3 interface and at the sample surface indicating that surfaces and interfaces strongly influence the overall Li diffusion kinetics. The accumulation of Li at the EUROFER/ Al_2O_3 substrate can be explained by considering that interfaces act as diffusion energy barriers for Li [40–43] and that some elements preferentially segregate to interfaces [40]. In addition to the previously discussed, another possible reason for having more Li at the coating surface could be the presence of residual Li that remains on the surface after exposure to PbLi, despite the cleaning process. This hypothesis is also compatible with the small color inhomogeneity observed in the coating surface after exposure to PbLi (see Fig. 1). Nevertheless, from our data, it is not possible to obtain information on the diffusivity or solubility of Li, neither in the Al_2O_3 nor in the EUROFER, since its determination requires to carry out measurements as a function temperature. A deeper study of the diffusion mechanisms of Li in these materials could be the subject of further work.

Based on the presented measured Li depth profiles, however, it is very relevant to discuss what the behavior of these coatings would be under real operation conditions in the breeder location in which, as previously mentioned, the coating will not only be subject to corrosion at high temperatures but also to neutron irradiation in a synergistic way. Therefore, in the following, we discuss the effect of irradiation at high temperature for Al_2O_3 coatings containing lithium after exposure to PbLi since the incorporation of lithium to the coating may have some important drawbacks in order to implement these coatings as TPBs, especially because of the neutron irradiation. On the one hand, according to Tanaka *et al.* neutron irradiation can produce Li recoil atoms from the liquid metal breeder [44] that can penetrate into the coating and/or in the structural material underneath. On the other hand, neutrons interact with Li leading to transmutation reactions in which T and

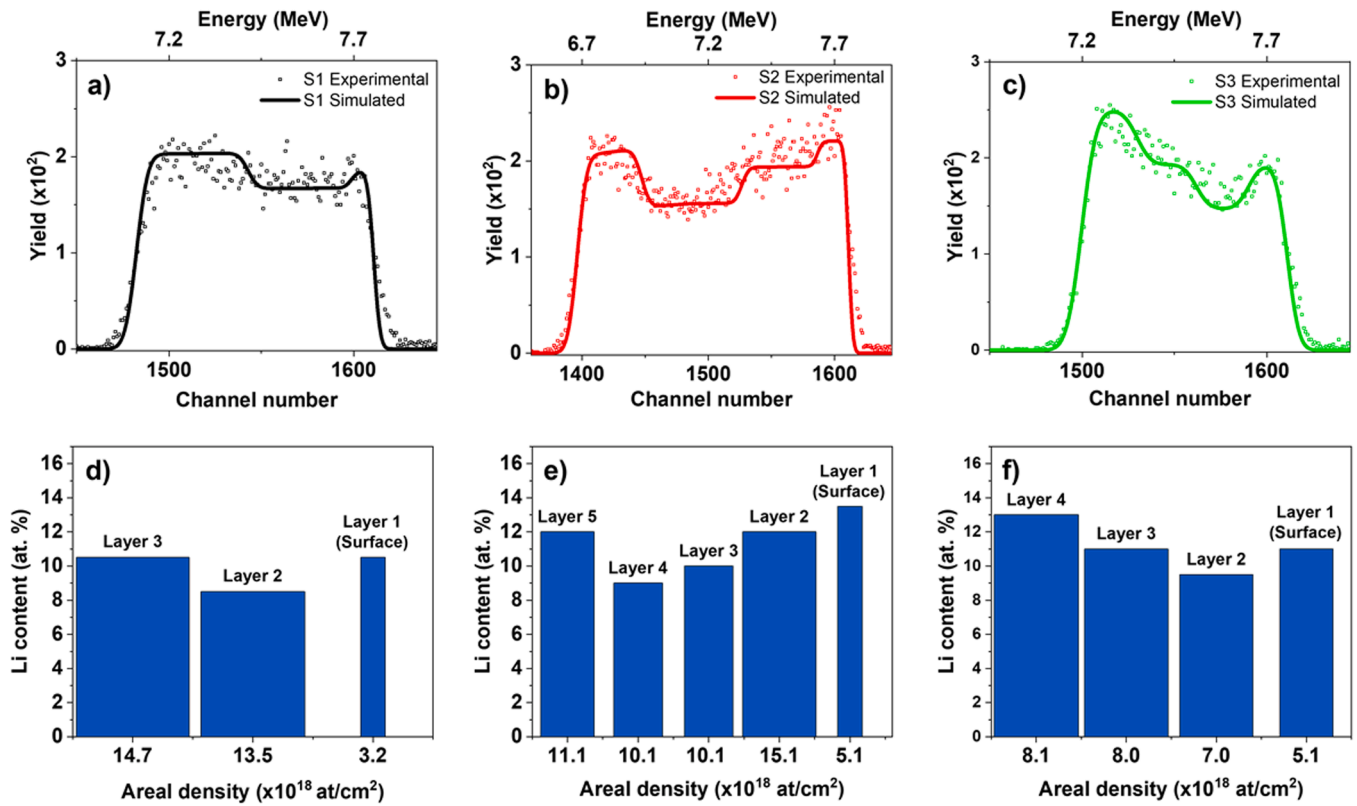


Fig. 5. Measured and simulated NRA spectra for three Al₂O₃ coatings after exposure to PbLi under the conditions described in Table I, together with the schematic representation of the calculated Li concentration in at.% and, areal density (at/cm²) of each particular layer in which the coatings have been divided to fit the measured spectra.

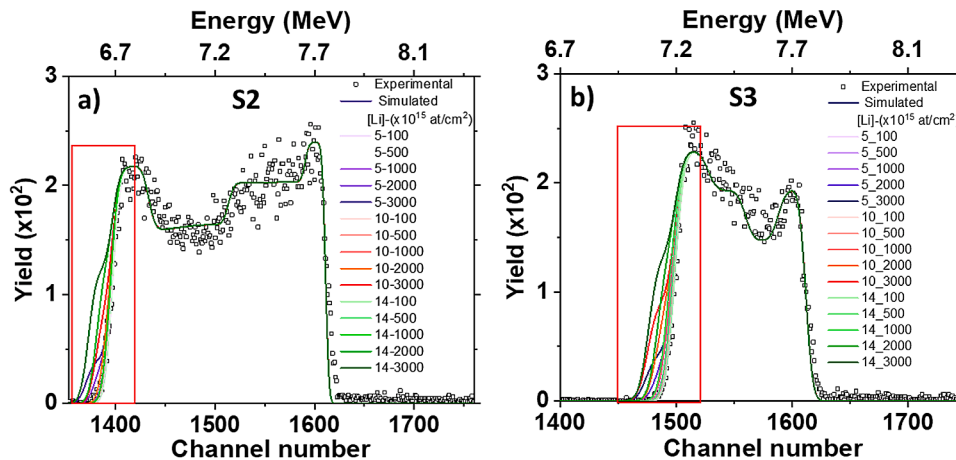


Fig. 6. Measured and simulated NRA spectra for two Al₂O₃ coatings with different thickness, 5 μm for S2, (a), and 2 μm for S3, (b), after exposure to PbLi under the conditions described in Table . For the simulation the Li contents were assumed to be 5, 10 and 14 at.% and the Li penetration depth was increased from 100 × 10¹⁵ to 3000 10¹⁵ at/cm².

He are produced according to the following reaction:



The consequences of He and T generation in the coating performance will strongly depend on the behavior of amorphous Al₂O₃ coatings under the combined effect of high temperature (500 °C) and neutron irradiation. Thus, on the final structure of the coating as well as, on the radiation induced defects (vacancies and interstitials) if any. To the best of our knowledge, this behavior has been poorly investigated for amorphous Al₂O₃.

First, we start to analyze the effect of temperature. In principle, at temperatures close to that for the BB operation (550 °C), amorphous Al₂O₃ starts to nucleate and to undergo transition to the metastable γ-δ-θ phases [45,46]. Aluminum oxide phase transformations are accompanied by changes in symmetry that lead to a modification of volume [46], which could risk the coating integrity. However, in our particular case, given the high density of the coating, phase transformations due to long-term temperature exposure do not seem very likely: the coatings are expected to remain amorphous. However, if not only temperature effects are considered but also the radiation environment in the BB, the

situation will be different, because diverse authors have shown that irradiation of similar coatings, under certain conditions, can also produce recrystallization. e. g. Zaborowska et al. report that amorphous Al_2O_3 coatings with a thickness of 1 μm deposited on 316 L stainless steel by Pulsed Laser Deposition (PLD) irradiated with 1.2 MeV Au^+ ions at room temperature up to 25 displacements per atom (dpa) remain amorphous without presenting any evidence of void formation, segregation of elements or crystallization [47] but at larger fluences (39 dpa) irradiation promotes the formation of voids and an amorphous-to-crystalline transformation resulting in a fully nano-grained structure. Crystallization is also observed for similar coatings irradiated at higher temperatures (600 °C) with 12 MeV Au^{5+} ions and 18 MeV W^{8+} ions from 20 to 150 dpa [48]. The crystalline phases present in the irradiated coatings depend on the radiation damage being the $\gamma\text{-Al}_2\text{O}_3$ up to 40 dpa, and both $\gamma\text{-Al}_2\text{O}_3$ and $\alpha\text{-Al}_2\text{O}_3$ for coatings irradiated at 150 dpa. The grain growth has been observed to increase with rising of the irradiation fluence and/or the irradiation temperature [48, 49]. Thus, at typical breeder fluences and operation temperature amorphous coatings are expected to become nanocrystalline.

As it happens in many other materials, grain boundaries (GBs) could govern the material performance under irradiation by playing a crucial role in the light species behavior and in the dynamics of interstitials and/or vacancies which also interact with light species i. e. vacancies can trap light species [50–55]. Thus, GBs influence the behavior of light species by acting as trapping sites or effective diffusion channels for them and by influencing the dynamic of interstitials and vacancies. The interaction of light species with GBs and radiation-induced defects is very complex since it depends, among other factors, on the light species itself (H-isotopes or He), the GB configuration and density, the properties (morphology, microstructure, type and number of native defects, etc.) of the material under study and the irradiation conditions (e.g., temperature, flux and fluence) [56–58]. Deuterium permeation experiments carried out in an amorphous Al_2O_3 coating irradiated with 6 MeV Au^{2+} ions at RT up to 39 dpa show that irradiation promotes the diffusion of deuterium atoms, increasing the coating permeability and decreasing its permeation reduction factor (PRF) [59]. Concerning He, experimental and computer simulation data indicate that below 800 K, amorphous Al_2O_3 has a large capacity for He retention since He atoms can be easily trapped in local potential wells. However, He retention strongly decreases when Al_2O_3 crystallizes [60]. Thus, in agreement with some other works reported in literature these results indicate that GBs could also behave as effective diffusion channels for He via a complex mechanism [61].

The diffused D and He in the coating after irradiation could penetrate into the EUROFER leading to embrittlement, or they can accumulate at the Al_2O_3 /EUROFER interface promoting the detachment of the coating. Besides, the diffusion of T could hinder the control of its inventory in the reactor, which is very undesirable from the safety point of view.

So far, experiments have been performed to study the behavior of H-isotopes or He. However, in order to have a good estimate of the coating behavior under realistic operation conditions in the breeder location, in which T and He will be produced simultaneously, one has also to consider that He atoms or clusters probably affect the H-isotope diffusion. For example, He-point defects complex has been reported to increase the activation energy of H migration in $\alpha\text{-Al}_2\text{O}_3$ [62]. Therefore, from previously reported data we can only speculate about the consequences of having light species in the Al_2O_3 coatings. Further research is needed in order to arrive to proper conclusions.

5. Conclusions

The Li content and distribution as a function of depth have been investigated by SIMS and a combination of IBA techniques (NRA and RBS) for amorphous, dense and well adhered to the substrate Al_2O_3 coatings after exposed to PbLi at a temperature of 550 °C for up to 7000 h under stagnant conditions. SIMS and IBA data show that Li diffuses

along the whole coating thickness, being the Li content larger at the coating surface and at the coating/EUROFER interface than at any other point within the coating. Li contents of up to 14 at.% were calculated in the coating region close to coating/EUROFER interface.

Under neutron irradiation, Li will transmute into He and T which could have some important drawbacks in the application of Al_2O_3 as TPBs both from the safety and from the technological point of view.

The data presented here are the input data needed to accurately calculate the light species inventory produced out of the Li content reported in this paper for Al_2O_3 coatings in contact with PbLi. The calculation of this inventory in turn allows to dictate the experimental conditions needed to simulate the coating behavior under realistic irradiation conditions.

CRedit

R. González-Arrabal Conceptualization (lead), investigation (equal), formal analysis (equal) validation (equal), visualization (equal), writing (lead) review and editing (lead); **E. Carella** Conceptualization (supporting), investigation (equal), validation (equal) writing-review and editing (equal); **F. J. Sánchez** Conceptualization (supporting), investigation (equal), validation (equal), visualization (equal), formal analysis (equal) writing review and editing (equal); **G. de la Cuerda-Velázquez** formal analysis (equal), validation (supporting), visualization (equal), writing review (equal) and editing (lead); **G. García** Conceptualization (supporting), investigation (equal), writing review and editing (equal); **J. M. Perlado** review (equal); **T. Hernández** Conceptualization (supporting), investigation (equal), validation (equal), visualization (equal), formal analysis (equal) writing review and editing (equal).

Declaration of Competing Interest

The authors declare the following financial interests/personal relationships which may be considered as potential competing interests: Raquel Gonzalez-Arrabal reports financial support was provided by Ministerio de Ciencia e Innovación, Comunidad de Madrid, European Union.

Data availability

Data will be made available on request.

Acknowledgments

This work has been carried out within the framework of the EUROfusion Consortium and has received funding from the Euratom research and training program 2014–2018 and 2019–2020 under grant agreement No 633053. “The views and opinions expressed herein do not necessarily reflect those of the European Commission.” This work has been supported by MICINN Projects (Ministerio de Ciencia e Innovación) PID2019–105325RB-C31 and PID2019–105325RB-C32 and TechnoFusion Project (P2018/EMT- 4437) of the CAM (Comunidad Autónoma Madrid) and acknowledges the Convenio Plurianual con la Universidad Politécnica de Madrid en la línea de actuación Programa de Excelencia para el Profesorado Universitario of the CAM for the financial support. It also was partially funded under Eurofusion Enable Research CfP-FSD-AWP21-ENR-01 (2021–2025) and ENR-IFE19.CCFE-01 (2019–2020) and Horizon EURATOM-2021-NRT-01 project 101059408. G. de La Cuerda-Velázquez acknowledges la Catedra de Seguridad Nuclear “Federico Goded” for the financial support.

The authors acknowledge the support from The Centro de Microanálisis de Materiales (CMAM)—Universidad Autónoma de Madrid, for the beam time proposals with codes STD044/21, STD006/22 and STD009/22, and its technical staff for their contribution to the operation

of the accelerator.

References

- [1] J. Konys, W. Krauss, Z. Voss, O. Wedemeyer, Corrosion behavior of EUROFER steel in flowing eutectic Pb–17Li alloy, *J. Nucl. Mater.* 329–333 (2004) 1379–1383, <https://doi.org/10.1016/j.jnucmat.2004.04.302>.
- [2] J. Konys, W. Krauss, H. Steiner, J. Novotny, A. Skrypnik, Flow rate dependent corrosion behavior of Eurofer steel in Pb–15.7Li, *J. Nucl. Mater.* 417 (2011) 1191–1194, <https://doi.org/10.1016/j.jnucmat.2010.12.277>.
- [3] G. Ilinčev, D. Kárník, M. Paulovic, A. Doubková, The effect of temperature and oxygen content on the flowing liquid metal corrosion of structural steels in the Pb–Bi eutectic, *Nucl. Eng. Des.* 236 (2006) 1909–1921, <https://doi.org/10.1016/j.nucengdes.2006.02.003>.
- [4] V. Tsisar, C. Schroer, O. Wedemeyer, A. Skrypnik, J. Konys, Corrosion interaction of 9%Cr ferritic/martensitic steels at 450 and 550°C with flowing Pb–Bi eutectic containing 10–7 Mass% dissolved oxygen, *J. Nucl. Eng. Radiat. Sci.* 5 (2019), <https://doi.org/10.1115/1.4041432>.
- [5] C. Shan, A. Wu, Q. Chen, The behavior of diffusion and permeation of tritium through 316L stainless steel, *J. Nucl. Mater.* 179–181 (1991) 322–324, [https://doi.org/10.1016/0022-3115\(91\)90091-K](https://doi.org/10.1016/0022-3115(91)90091-K).
- [6] T. Tanabe, Tritium fuel cycle in ITER and DEMO: issues in handling large amount of fuel, *J. Nucl. Mater.* 438 (2013) S19–S26, <https://doi.org/10.1016/j.jnucmat.2013.01.284>.
- [7] E. Malitckii, Hydrogen and helium effects on reduced activation Fe–Cr ferrite–martensite and ODS steels, (n.d.) <https://aaltodoc.aalto.fi/bitstream/handle/123456789/18522/isbn9789526065403.pdf?sequence=1>.
- [8] Y. Yagodzinskyy, E. Malitckii, M. Ganchenkova, S. Binyukova, O. Emelyanova, T. Saukkonen, H. Hänninen, R. Lindau, P. Vladimirov, A. Moeslang, Hydrogen effects on tensile properties of EUROFER 97 and ODS-EUROFER steels, *J. Nucl. Mater.* 444 (2014) 435–440, <https://doi.org/10.1016/j.jnucmat.2013.10.026>.
- [9] E.C.E. Rönnebro, R.L. Oelrich, R.O. Gates, Recent advances and prospects in design of hydrogen permeation barrier materials for energy applications—a review, *Molecules* 27 (2022) 6528, <https://doi.org/10.3390/molecules27196528>.
- [10] M. Utili, S. Bassini, S. Cataldo, F. Di Fonzo, M. Kordac, T. Hernandez, K. Kunzova, J. Lorenz, D. Martelli, B. Padino, A. Moroño, M. Tarantino, C. Schroer, G. A. Spagnuolo, L. Vala, M. Vanazzi, A. Venturini, Development of anti-permeation and corrosion barrier coatings for the WCLL breeding blanket of the European DEMO, *Fusion Eng. Des.* 170 (2021), 112453, <https://doi.org/10.1016/j.fusengdes.2021.112453>.
- [11] J. Konys, A. Aiello, G. Benamati, L. Giancarli, Status of tritium permeation barrier development in the EU, *Fusion Sci. Technol.* 47 (2005) 844–850, <https://doi.org/10.13182/FST05-A791>.
- [12] A. Houben, M. Rasiński, L. Gao, Ch. Linsmeier, Tungsten nitride as tritium permeation barrier, *Nucl. Mater. Energy* 24 (2020), 100752, <https://doi.org/10.1016/j.nme.2020.100752>.
- [13] K.S. Forcey, A. Perujo, Tritium permeation barriers in contact with liquid lithium–lead eutectic (Pb–17Li), JRC Publ. Reposit. (1995). <https://publications.jrc.ec.europa.eu/repository/handle/JRC11336>.
- [14] R.A. Causey, R.A. Karnesky, C. San Marchi, 4.16 - tritium barriers and tritium diffusion in fusion reactors, in: R.N.J. Konings (Ed.), *Comprehensive Nuclear Materials*, Elsevier, Oxford, 2012, pp. 511–549, <https://doi.org/10.1016/B978-0-08-056033-5.00116-6>.
- [15] D. Levchuk, H. Bolt, M. Döbeli, S. Eggenberger, B. Widrig, J. Ramm, Al–Cr–O thin films as an efficient hydrogen barrier, *Surf. Coat. Technol.* 202 (2008) 5043–5047, <https://doi.org/10.1016/j.surfcoat.2008.05.012>.
- [16] D. Stöver, H.P. Buchkremer, R. Hecker, Hydrogen and deuterium permeation through metallic and surface-oxidized chromium, *Surf. Coat. Technol.* 28 (1986) 281–290, [https://doi.org/10.1016/0257-8972\(86\)90085-X](https://doi.org/10.1016/0257-8972(86)90085-X).
- [17] T. Hernández, A. Moroño, F.J. Sánchez, C. Maffiotte, M.A. Monclús, R. González-Arrabal, Study of deuterium permeation, retention, and desorption in SiC coatings submitted to relevant conditions for breeder blanket applications: thermal cycling effect under electron irradiation and oxygen exposure, *J. Nucl. Mater.* 557 (2021), 153219, <https://doi.org/10.1016/j.jnucmat.2021.153219>.
- [18] T. Hernández, F.J. Sánchez, F. Di Fonzo, M. Vanazzi, M. Panizo, R. González-Arrabal, Corrosion protective action of different coatings for the helium cooled pebble bed breeder concept, *J. Nucl. Mater.* 516 (2019) 160–168, <https://doi.org/10.1016/j.jnucmat.2019.01.009>.
- [19] T. Hernández, F.J. Sánchez, A. Moroño, E. León-Gutiérrez, M. Panizo-Laiz, M. A. Monclús, R. González-Arrabal, Corrosion behavior of diverse sputtered coatings for the helium cooled pebbles bed (HCPB) breeder concept, *Nucl. Mater. Energy* 25 (2020), 100795, <https://doi.org/10.1016/j.nme.2020.100795>.
- [20] R. Petráš, K. Kunzová, A. Fedoriková, J. Kekt, M. Kordac, F. Di Fonzo, B. Paladino, C. Schroer, J. Lorenz, M. Utili, L. Vala, Characterization of aluminum-based coatings after short term exposure during irradiation campaign in the LVR-15 fission reactor, *Fusion Eng. Des.* 170 (2021), 112521, <https://doi.org/10.1016/j.fusengdes.2021.112521>.
- [21] P. Muñoz, T. Hernández, I. García-Cortés, F.J. Sánchez, A. Maira, D. Iadicicco, M. Vanazzi, M. Utili, F. Di Fonzo, A. Moroño, Radiation effects on deuterium permeation for PLD alumina coated Eurofer steel measured during 1.8 MeV electron irradiation, *J. Nucl. Mater.* 512 (2018) 118–125, <https://doi.org/10.1016/j.jnucmat.2018.10.008>.
- [22] H.A. Horan, J.B. Damiano, The Formation and Composition of Lithium Aluminate, ACS Publications, 2002, <https://doi.org/10.1021/ja01315a033>.
- [23] N.I. Jamnapara, A. Sarada Sree, E. Rajendra Kumar, S. Mukherjee, A.S. Khanna, Compatibility study of plasma grown alumina coating with Pb–17Li under static conditions, *J. Nucl. Mater.* 455 (2014) 612–617, <https://doi.org/10.1016/j.jnucmat.2014.08.046>.
- [24] B.A. Pint, K.L. More, Transformation of Al₂O₃ to LiAlO₂ in Pb–17Li at 800°C, *J. Nucl. Mater.* 376 (2008) 108–113, <https://doi.org/10.1016/j.jnucmat.2007.12.010>.
- [25] G.C. Wilson, J.V.P. Long, SIMS analysis of lithium: ion implantation and matrix effects, *Int. J. Mass Spectrom. Ion Phys.* 42 (1982) 63–75, [https://doi.org/10.1016/0020-7381\(82\)80053-3](https://doi.org/10.1016/0020-7381(82)80053-3).
- [26] K. Kanamura, S. Shiraishi, H. Takezawa, Z. Takehara, XPS analysis of the surface of a carbon electrode intercalated by lithium ions, *Chem. Mater.* 9 (1997) 1797–1804, <https://doi.org/10.1021/cm970042v>.
- [27] J. Maier, B. Pfeiffer, C.A. Volkert, C. Nowak, Three-dimensional microstructural characterization of lithium manganese oxide with atom probe tomography, *Energy Technol.* 4 (2016) 1565–1574, <https://doi.org/10.1002/ente.201600210>.
- [28] S. Bassini, Coolant Chemistry Control in Heavy Liquid Metal Cooled Nuclear Systems, Doctoral Thesis, Alma Mater Studiorum - Università di Bologna, 2017, <https://doi.org/10.6092/unibo/amsdottorato/802.6>.
- [29] F. García Ferré, M. Ormellese, F. Di Fonzo, M.G. Beghi, Advanced Al₂O₃ coatings for high temperature operation of steels in heavy liquid metals: a preliminary study, *Corros Sci* 77 (2013) 375–378, <https://doi.org/10.1016/j.corsci.2013.07.039>.
- [30] A. Redondo-Cubero, M.J.G. Borge, N. Gordillo, P.C. Gutiérrez, J. Olivares, R. Pérez Casero, M.D. Ynsa, Current status and future developments of the ion beam facility at the centre of micro-analysis of materials in Madrid, *Eur. Phys. J. Plus.* 136 (2021) 175, <https://doi.org/10.1140/epjp/s13360-021-01085-9>.
- [31] R. González-Arrabal, M. Panizo-Laiz, K. Fujita, K. Mima, A. Yamazaki, T. Kamiya, Y. Orikasa, Y. Uchimoto, H. Sawada, C. Okuda, Y. Kato, J.M. Perlado, Meso-scale characterization of lithium distribution in lithium-ion batteries using ion beam analysis techniques, *J. Power Sources* 299 (2015) 587–595, <https://doi.org/10.1016/j.jpowsour.2015.09.022>.
- [32] J.F. Ziegler, M.D. Ziegler, J.P. Biersack, SRIM – the stopping and range of ions in matter (2010), *Nucl. Instrum. Methods Phys. Res., Sect. B* 268 (2010) 1818–1823, <https://doi.org/10.1016/j.nimb.2010.02.091>.
- [33] P. Sebayang, Nurdina, S. Simbolon, C. Kurmiawan, M. Yunus, E.A. Setiadi, Z. Sitorus, Fabrication and characterization of fine ceramic based on alumina, bentonite, and glass bead, *J. Phys.: Conf. Ser.* 985 (2018), 012024, <https://doi.org/10.1088/1742-6596/985/1/012024>.
- [34] A. Sagara, K. Kamada, S. Yamaguchi, Depth profiling of lithium by use of the nuclear reaction ⁷Li(p, α)⁴He, *Nucl. Instrum. Methods Phys. Res., Sect. B* 34 (1988) 465–469, [https://doi.org/10.1016/0168-583X\(88\)90151-6](https://doi.org/10.1016/0168-583X(88)90151-6).
- [35] M. Mayer, www.simnra.com.
- [36] V. Paneta, A. Kafkarkou, M. Kokkoris, A. Lagoyannis, Differential cross-section measurements for the ⁷Li(p,p₀)⁷Li, ⁷Li(p,p₁)⁷Li, ⁷Li(p,α₀)⁴He, ¹⁹F(p,p₀)¹⁹F, ¹⁹F(p,α₀)¹⁶O and ¹⁹F(p,α_{1,2})¹⁶O reactions, *Nucl. Instrum. Methods Phys. Res., Sect. B* 288 (2012) 53–59, <https://doi.org/10.1016/j.nimb.2012.07.020>.
- [37] Pier A.de Groot, Chapter 2 - Lithium. Handbook of Stable Isotope Analytical Techniques, Elsevier, Amsterdam, 2009, p. 225, <https://doi.org/10.1016/B978-0-444-51115-7.00002-4>.
- [38] S. Hao, C. Wolverson, Lithium transport in amorphous Al₂O₃ and AlF₃ for discovery of battery coatings, *J. Phys. Chem. C* 117 (2013) 8009–8013, <https://doi.org/10.1021/jp311982d>.
- [39] A. Van der Ven, J.C. Thomas, Q. Xu, B. Swoboda, D. Morgan, Nondilute diffusion from first principles: Li diffusion in Li_xTiS₂, *Phys. Rev. B* 78 (2008), 104306, <https://doi.org/10.1103/PhysRevB.78.104306>.
- [40] P. Wynnblatt, V. Ghetta, D. Gorse, D. Mazière, V. Pontikis, Materials Issues for Generation IV Systems, Introduction to interfaces and diffusion. NATO Science for Peace and Security Series B: Physics and Biophysics, Springer Netherlands, Dordrecht, 2008, pp. 393–424, https://doi.org/10.1007/978-1-4020-8422-5_20.
- [41] J. Shi, Z. Wang, Y.Q. Fu, Density functional theory study of lithium diffusion at the interface between olivine-type LiFePO₄ and LiMnPO₄, *J. Phys. D: Appl. Phys.* 49 (2016), 505601, <https://doi.org/10.1088/0022-3727/49/5/050601>.
- [42] M. Liu, C. Wang, C. Zhao, E. van der Maas, K. Lin, V.A. Arszewska, B. Li, S. Ganapathy, M. Wagemaker, Quantification of the Li-ion diffusion over an interface coating in all-solid-state batteries via NMR measurements, *Nat. Commun.* 12 (2021) 5943, <https://doi.org/10.1038/s41467-021-26190-2>.
- [43] P. Benedek, O.K. Forslund, E. Nocerino, N. Yazdani, N. Matsubara, Y. Sassa, F. Jaglinski, M. Medarde, M. Telling, M. Månsson, V. Wood, Quantifying diffusion through interfaces of lithium-ion battery active materials, *ACS Appl. Mater. Interfaces* 12 (2020) 16243–16249, <https://doi.org/10.1021/acsaami.9b21470>.
- [44] T. Tanaka, T. Chikada, T. Hinoki, T. Muroga, Electrical insulation performances of ceramic materials developed for advanced blanket systems under intense radiations, *J. Nucl. Mater.* 569 (2022), 153917, <https://doi.org/10.1016/j.jnucmat.2022.153917>.
- [45] I. Levin, D. Brandon, Metastable alumina polymorphs: crystal structures and transition sequences, *J. Am. Ceram. Soc.* 81 (1998) 1995–2012, <https://doi.org/10.1111/j.1151-2916.1998.tb02581.x>.
- [46] R.-S. Zhou, R.L. Snyder, Structures and transformation mechanisms of the η, γ and θ transition allotropes, *Acta Crystallographica Sect. B* 47 (1991) 617–630, <https://doi.org/10.1107/S0108768191002719>.
- [47] A. Zaborowska, Ł. Kurpaska, M. Clozel, E.J. Olivier, J.H. O’Connell, M. Vanazzi, F. Di Fonzo, A. Azarov, I. Jóźwik, M. Frelek-Kozak, R. Diduszko, J.H. Neethling, J. Jagielski, Absolute radiation tolerance of amorphous alumina coatings at room temperature, *Ceram. Int.* 47 (2021) 34740–34750, <https://doi.org/10.1016/j.ceramint.2021.09.013>.

- [48] F. García Ferré, A. Mairov, L. Ceseracciu, Y. Serruys, P. Trocellier, C. Baumier, O. Kaïtasov, R. Brescia, D. Gastaldi, P. Vena, M.G. Beghi, L. Beck, K. Sridharan, F. Di Fonzo, Radiation endurance in Al₂O₃ nanoceramics, *Sci. Rep.* 6 (2016) 33478, <https://doi.org/10.1038/srep33478>.
- [49] N. Yu, M. Nastasi, Ion beam induced epitaxial recrystallization of alumina thin films deposited on sapphire, *Nucl. Instrum. Methods Phys. Res., Sect. B* 106 (1995) 579–582, [https://doi.org/10.1016/0168-583X\(95\)00773-3](https://doi.org/10.1016/0168-583X(95)00773-3).
- [50] R. Gonzalez-Arrabal, M. Panizo-Laiz, N. Gordillo, E. Tejado, F. Munnik, A. Rivera, J.M. Perlado, Hydrogen accumulation in nanostructured as compared to the coarse-grained tungsten, *J. Nucl. Mater.* 453 (2014) 287–295, <https://doi.org/10.1016/j.jnucmat.2014.06.057>.
- [51] S.J. Zinkle, Effect of H and He irradiation on cavity formation and blistering in ceramics, *Nucl. Instrum. Methods Phys. Res., Sect. B* 286 (2012) 4–19, <https://doi.org/10.1016/j.nimb.2012.03.030>.
- [52] J. Chen, Z.Y. He, P. Jung, Microstructure of helium-implanted α -Al₂O₃ after annealing, *Acta Mater.* 54 (2006) 1607–1614, <https://doi.org/10.1016/j.actamat.2005.11.030>.
- [53] A. van Veen, R.J.M. Konings, A.V. Fedorov, Helium in inert matrix dispersion fuels, *J. Nucl. Mater.* 320 (2003) 77–84, [https://doi.org/10.1016/S0022-3115\(03\)00173-9](https://doi.org/10.1016/S0022-3115(03)00173-9).
- [54] R. Gonzalez-Arrabal, A. Rivera, J.M. Perlado, Limitations for tungsten as plasma facing material in the diverse scenarios of the European inertial confinement fusion facility HiPER: current status and new approaches, *Matter Radiat. Extremes* 5 (2020), 055201, <https://doi.org/10.1063/5.0010954>.
- [55] G. Valles, M. Panizo-Laiz, C. González, I. Martín-Bragado, R. González-Arrabal, N. Gordillo, R. Iglesias, C.L. Guerrero, J.M. Perlado, A. Rivera, Influence of grain boundaries on the radiation-induced defects and hydrogen in nanostructured and coarse-grained tungsten, *Acta Mater.* 122 (2017) 277–286, <https://doi.org/10.1016/j.actamat.2016.10.007>.
- [56] M. Panizo-Laiz, P. Díaz-Rodríguez, A. Rivera, G. Valles, I. Martín-Bragado, J. M. Perlado, F. Munnik, R. González-Arrabal, Experimental and computational studies of the influence of grain boundaries and temperature on the radiation-induced damage and hydrogen behavior in tungsten, *Nucl. Fusion.* 59 (2019), 086055, <https://doi.org/10.1088/1741-4326/ab26e9>.
- [57] D. Fernández-Pello, M.A. Cerdeira, J. Suárez-Recio, R. González-Arrabal, R. Iglesias, C. González, Coexistence of a self-interstitial atom with light impurities in a tungsten grain boundary, *J. Nucl. Mater.* 560 (2022), 153481, <https://doi.org/10.1016/j.jnucmat.2021.153481>.
- [58] F. Wang, W.-S. Lai, R.-S. Li, B. He, S.-F. Li, Interactions between vacancies and prismatic $\Sigma 3$ grain boundary in α -Al₂O₃: first principles study*, *Chinese Phys. B.* 25 (2016), 066804, <https://doi.org/10.1088/1674-1056/25/6/066804>.
- [59] W. Zhang, J. Deng, C. Zhu, Y. Zhong, J. Yang, H. Xin, G. Liu, R. Tang, K. Feng, N. Liu, J. Yang, Au-ion irradiation effects on microstructure and deuterium permeation resistance of Al/Al₂O₃ coating, *Nucl. Fusion.* 62 (2022), 086039, <https://doi.org/10.1088/1741-4326/ac74d0>.
- [60] S. Zhang, E. Yu, S. Gates, W.S. Cassata, J. Makel, A.M. Thron, C. Bartel, A. W. Weimer, R. Faller, P. Stroeve, J.W. Tringe, Helium interactions with alumina formed by atomic layer deposition show potential for mitigating problems with excess helium in spent nuclear fuel, *J. Nucl. Mater.* 499 (2018) 301–311, <https://doi.org/10.1016/j.jnucmat.2017.11.029>.
- [61] F. Wang, W. Lai, R. Li, B. He, S. Li, Vacancy-enhanced mechanism for helium diffusion along $\Sigma 7$ grain boundary in α -Al₂O₃: a first principle study, nuclear instruments and methods in physics research section b: beam interactions with materials and atoms. 393 (2017) 88–92. doi: <https://doi.org/10.1016/j.nimb.2016.11.022>.
- [62] G. Zhang, X. Xiang, F. yang, X. peng, T. Tang, Y. Shi, X. Wang, Helium stability and its interaction with H in α -Al₂O₃: a first-principles study, *Phys. Chem. Chem. Phys.* (2015) 18, <https://doi.org/10.1039/C5CP06496A>.